In situ surface functionalization of magnetic nanoparticles with hydrophilic natural amino acids

Article *in* Inorganica Chimica Acta · July 2012

DOI: 10.1016/j.ica.2012.01.058

CITATIONS
41

READS
619

4 authors, including:

Haiou Qu
U.S. Food and Drug Administration
28 PUBLICATIONS **986** CITATIONS

SEE PROFILE

Inorganica Chimica Acta 389 (2012) 60–65

Contents lists available at SciVerse ScienceDirect

Inorganica Chimica Acta

journal homepage: www.elsevier.com/locate/ica

In situ surface functionalization of magnetic nanoparticles with hydrophilic natural amino acids

Haiou Qu [a,b], Hui Ma [a,b], Weilie Zhou [b], Charles J. O'Connor [a,b,*]

[a] Department of Chemistry, University of New Orleans, 2000 Lakeshore Dr., New Orleans, LA, USA
[b] Advanced Materials Research Institute, University of New Orleans, 2000 Lakeshore Dr., New Orleans, LA, USA

ARTICLE INFO

Article history:
Available online 15 February 2012

Dedicated to Prof. Jon Zubieta

Keywords:
Iron oxide nanoparticles
Surface functionalization
Ligand exchange
Amino acids

ABSTRACT

The surface of magnetic iron oxide nanoparticles has been modified with hydrophilic natural amino acids via an *in situ* method. A rapid ligand exchange reaction was induced at elevated temperatures to replace the original labile solvent layer with amino acids. The functionalized nanoparticles were quasi-spherical and well separated with an average diameter around 7 nm. The resulted products were examined to be highly crystalline and phase-pure Fe_3O_4. The present of amino acids on the surface of the nanoparticles was verified by Fourier transform infrared spectroscopy and X-ray photoelectron spectroscopy, which indicated successful ligand exchange. Zeta potential and dynamic light scattering measurement suggested that functionalized magnetic nanoparticles were well dispersed in both basic and acidic aqueous solution with small polydispersity. The uncoordinated amine groups are highly reactive and available for either conjugation with biocompatible polymers or attachment of small gold nanocrystals, so as to prepare dual-functional nanocomposite.

1. Introduction

Magnetic iron oxide nanoparticles are of great interest to researchers in biomedical areas such as magnetic resonance imaging (MRI) [1], magnetically controlled target delivery [2] and bioseparations [3] because of their biocompatibility and magnetic properties. The thermal decomposition of different iron precursors in non-polar, high boiling point solvents in the presence of a reducing agent can yield high quality monodispersed magnetic nanoparticles without any size selection process [4–6]. Monofunctional fatty acid, amine or alcohol molecules such as oleic acid, oleylamine and oleylalcohol are usually used as capping agents for surface passivation and stabilization of the nanocrystals in nonpolar solvents. However, ascribed to the hydrophobicity and limited reactivity of these molecules, sophisticated postsynthetic functionalization is required so that the nanoparticles can be dispersed in aqueous solution and sustain a secondary reaction for further modification [7].

The most common surface functionalization approach is a low temperature ligand exchange reaction, where the original ligand shell is exposed to excessive amounts of competing capping ligand [8,9] followed by precipitation and isolation. Although, a wide variety of functionalities can be immobilized onto the surface of nanoparticles, and repeating the cycle above allows more thorough replacement, relatively low product yield and decreased stability after the exchange remain issues with this method.

Despite efforts to develop more efficient modification methods, the stabilization of iron oxide nanoparticles in different solvents is another major concern during functionalization. Choosing an appropriate capping ligand molecule is crucial to obtain nanoparticles with good stability since these stabilizers are responsible for generating inter-particles repulsive force in order to prevent aggregations. Many small organic molecules and polymers such as citric acid [9], dopamine [10] and polyethylene glycol [11] have been tested as stabilizing agents for magnetic nanoparticles in aqueous solution. Among the candidates, natural amino acids (AA's) represent a unique class of small organic molecules with attractive properties for magnetic nanoparticle functionalization. Their low cost, good biocompatibility and available functional groups for binding make them an ideal choice as capping ligand to stabilize magnetic nanoparticles in physiological conditions. In addition, besides amine and carboxylic groups at α position, many AA's possess additional functional groups such as guanidine, thiol and phenolic hydroxyl groups which are potential reaction sites for further modification. Moreover, some AA's such as arginine and leucine would cause tumor shrinkage when reaching certain concentration levels [12]. So far, attempts have been made to prepare the iron oxide nanoparticles with AA functionalities [13–15]; their practical applications, however, are mainly limited by the poor solubility and dispersibility in aqueous solution after the functionalization.

* Corresponding author at: Advanced Materials Research Institute, University of New Orleans, 2000 Lakeshore Dr., New Orleans, LA, USA. Tel.: +1 504 280 6848; fax: +1 504 280 3185.
E-mail address: coconnor@uno.edu (C.J. O'Connor).

0020-1693/$ - see front matter © 2012 Elsevier B.V. All rights reserved.
doi:10.1016/j.ica.2012.01.058

In this study, we demonstrate a novel one-pot method that successfully integrates the synthesis of nanocrystals with a high temperature ligand exchange reaction. Six different hydrophilic AA's, glycine (Gly), alanine (Ala), serine (Ser), arginine (Arg), threonine (Thr) and lysine (Lys) were selected as capping ligand molecules. The effect on the morphology and properties of the nanoparticles from different AA's were evaluated by transmission electron microscopy (TEM), X-ray diffractometry (XRD), Fourier transform infrared spectroscopy (FT-IR), X-ray photoelectron spectroscopy (XPS) and superconducting quantum interference device (SQUID). The reactivity of uncoordinated functional groups was investigated through gold nanocrystal attachment and biocompatible polymers conjugation.

2. Experimental

2.1. Preparation of amino acids functionalized magnetic nanoparticles

All chemicals were used as received without any further purification. In a typical synthesis [16], 0.5 mmol (99.4 mg) of $FeCl_2{\cdot}4H_2O$, 1 mmol (270.3 mg) of $FeCl_3{\cdot}6H_2O$, and 20 g of DEG were subsequently added to an argon protected three neck flask. Separately, 4 mmol (160 mg) of NaOH was dissolved in 10 g diethylene glycol and added to the flask above. The mixture was then heated up to 220 °C and maintained at 220 °C for 2 h. Meanwhile, 1 mmol of AA molecules was dissolved in 400 μl H_2O and mixed with 5 g DEG. At the end of heating, this mixture was injected into the flask and then the system was cooled to room temperature. The solid product was magnetically isolated and washed five times with absolute ethanol to remove the excess of DEG and other chemicals. Finally, the particles were redispersed in deionized water (10 ml) to give a clear solution. For FT-IR and SQUID measurements, after extensively washing with ethanol, the solid part was dried under vacuum.

2.2. Preparation of Au–Fe_3O_4 nanocomposite

The synthesis of 2–3 nm gold nanoparticles was based on Duff et al. method [17]. In a typical experiment, 0.5 ml 1 M NaOH was diluted by 45 ml deionized water, then mixed with 1 ml tetrakis(hydroxymethyl)phosphonium chloride (THPC 80%) solution for 5 min. Then, 1.5 ml 1% $HAuCl_4$ solution was quickly added and the solution was further stirred for 5 min.

For gold attachment, 5 ml of colloidal gold nanoparticles solution was introduced into 2 ml water dispersion of Fe_3O_4 nanoparticles, and the mixture was stirred for 6 h. The solid product was magnetically separated and washed with deionized water for five times to remove excessive amount of gold particles. The final product was redispersed in ethanol or water by sonication.

2.3. Conjugation of biocompatible polymer to the surface of amino acids coated nanoparticles

In a 10 ml flask, 10 mg AA coated nanoparticles was dispersed in 2 ml nanopure water. Separately, 50 mg 1-ethyl-3-(3-dimethylaminopropyl)carbodiimide (EDC) and 20 mg carboxyl polyethylene glycol (PEG, Mw ~ 2000) were dissolved in 3 ml water. The solution was activated for 15 min under thorough mixing. Then, the activated PEG solution was transfer to the 2 ml nanoparticles dispersion and stirred for 6 h. The solid product was magnetically separated, washed with ethanol for five times to remove excess PEG and dried under vacuum.

2.4. Characterization

The structure and phase purity of the product were examined by X-ray diffractometry using a Phillips X'pert system equipped with a graphite monochromator (Cu Kα radiation, $\lambda = 1.54056$ Å). Size distribution, particles morphology and crystallinity were studied on a JEOL 2010 transmission electron microscope (TEM). Surface composition was examined by Thermo Nicolet Nexus 670 FT-IR machine in 650–4000 cm^{-1} region and Kratos AXIS 165 X-ray Photoelectron Spectroscope. Energy-dispersive X-ray analysis (EDS) was performed on a JEOL 2010 transmission electron microscope. The magnetic properties were measured by Quantum Design SQUID magnetometer (MPMS XL-7) in the temperature range 5–300 K. Inductively coupled plasma atomic emission spectroscopy (ICP-AES) were used to calculate the net weight of iron oxide. The colloidal stability was investigated by dynamic light scattering (DLS) and zeta potential measurement (DelsaNano C). The absorbance spectra were measured with a Varian Cary 500 UV–Vis Spectrophotometer.

3. Results and discussion

3.1. Morphology and phase purity

The synthesis and surface functionalization of iron oxide nanoparticles with AA's were performed in the same pot instead of conducting a separate ligand exchange reaction after purifying and isolating the nanoparticles from the synthesis medium. By carefully adjusting the chemical concentration and heating rate during the synthesis, we can control the nucleation and growth of the nanocrystals, which effectively yields narrow-size-distributed iron oxide nanocrystals. At the end of the synthesis, AA molecules were introduced by a rapid injection at elevated temperatures, which induced a fast ligand exchange reaction. Owing to the increased thermal energy at high temperatures and strong coordinating ability of carboxylic groups [18], AA molecules would quickly replace the labile solvent shell and stabilize the nanocrystals. Fig. 1 presents the TEM studies of as-prepared, AA coated iron oxide nanoparticles. As shown in the images, nanoparticles with different AA coatings are all well dispersed and narrowly distributed without obvious variation on the morphology. Although nanoparticles stabilized by Ala and Gly appeared limited inter-particle spacing because of the short length of the ligand molecules, no massive aggregation was found in any AA functionalized nanoparticles. Moreover, it was noticed that under similar particle concentration positively charged Lys and Arg protected iron oxide nanoparticles presented improved dispersibility comparing to other polar and nonpolar AA's (Fig. S2, Supporting information). It can be explained by the strongly protonated amine groups of Lys and Arg in aqueous solution, which largely increases the electrostatic repulsion. Furthermore, relatively longer carbon chains are able to generate more steric hindrance to enhance the separation among nanoparticles [19]. On the basis of measuring more than 200 nanoparticles, the average diameters are 6.9–7.2 nm with 17.2–20.9% standard deviation for functionalized iron oxide nanoparticles, implying AA variation did not affect the size and distribution of the nanoparticle (Table 1).

The high resolution TEM images shown in Fig. 1 demonstrate that each AA functionalized nanoparticle is a well-developed nanocrystal. Detailed crystal structure and phase purity were examined by powder XRD, and magnetic nanoparticles with different surface composition gave similar patterns which matched standard bulk magnetite (JCPDS No. 19-0629) with no other secondary iron oxide

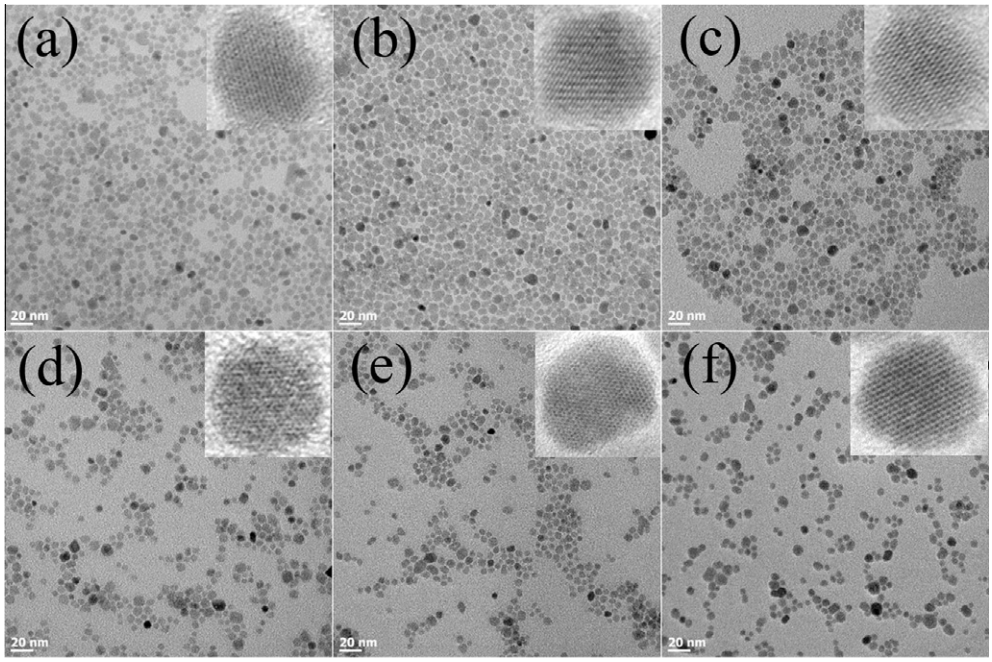

Fig. 1. TEM images of amino acid coated Fe_3O_4 nanoparticles. (Insets: high resolution TEM images of single magnetite nanoparticles.) (a) Ala, (b) Gly, (c) Ser, (d) Thr, (e) Lys, and (f) Arg.

Table 1
Size statistics and magnetic properties of magnetite nanocrystals capped with different amino acids.

Capping ligand	Size (nm)	SD[a] (%)	T_B (K)	H_c (Oe)	M_R[b] (emu g^{-1})	M_s (emu g^{-1})	M_n[c] (emu g^{-1})
Ala	7.2	17.6	77	288	12	60.6	75.2
Gly	7.0	20.9	77	290	16.5	63.2	77.2
Ser	7.1	18.6	69	300	16.9	60.5	75.6
Thr	6.9	18.1	74	292	14	65	78.7
Arg	7.1	20.7	80	294	13	57	76
Lys	7.0	17.2	74	272	13.7	62	78.3

[a] Standard deviation.
[b] Remanence.
[c] Normalized saturation magnetization.

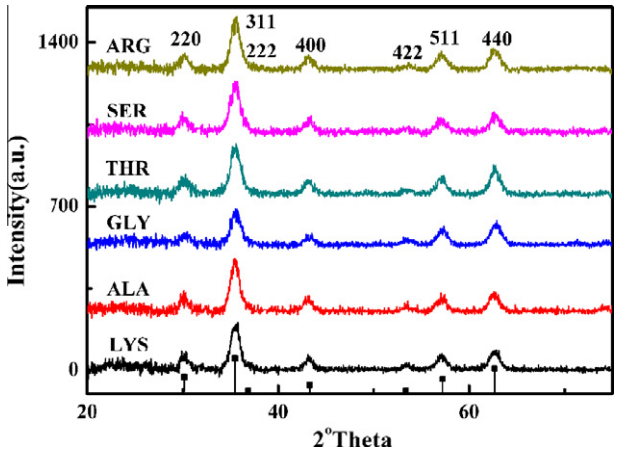

Fig. 2. XRD pattern of the amino acid coated Fe_3O_4 nanoparticles with the standard reference pattern of magnetite JCPDS No. 19-0629.

phases (Fig. 2). The calculated lattice constants are 8.390, 8.371, 8.390, 8.378, 8.379, 8.379 Å for Ala, Gly, Thr, Ser, Arg and Lys coated nanoparticles, respectively, which are very close to the lattice parameter of standard bulk magnetite (8.396 Å) and relatively far from the constant of maghemite (8.346 Å), indicating that AA functionalized iron oxide nanoparticles are magnetite.

3.2. Surface chemistry

Natural AA's share many similarities in their molecular structure such as carboxylic groups and amine groups at α position. Consequently, AA's coated nanoparticles showed similar spectra during FT-IR measurement (Fig. 3). More specifically, the characteristic vibrations of the carboxylic groups are located at 1410 and 1580 cm^{-1}, which are assigned to the symmetric and asymmetric COO– stretching. The difference between these two peaks is about 170 cm^{-1}, implying a bridging structure between the surface iron ions and carboxylic groups [20]. The absorption peaks at 1610 cm^{-1} which are overlapped with asymmetric COO– stretching corresponded to the N–H bending of amine groups. The weak peaks in 2800–3000 cm^{-1} region can be attributed to the C–H stretching of methyl or methylene groups. In addition, AA functionalized nanoparticles exhibit strong peaks near 1070 cm^{-1} ascribed to the C–OH stretching from DEG, which implies an incomplete replacement of original DEG with AA's during the ligand exchange. Functionalized iron oxide nanoparticles also exhibit a strong peak at 630 and 585 cm^{-1} which are assigned to the Fe–O vibration [21], indicating a covalent bond between capping li-

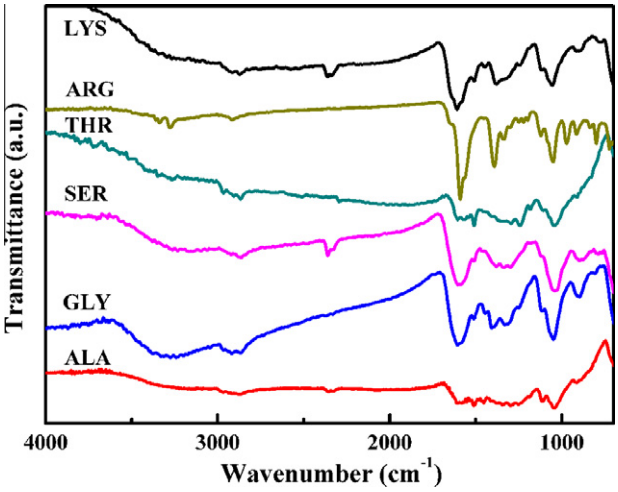

Fig. 3. FT-IR spectra of Fe_3O_4 nanoparticles with different capping ligands.

gand molecules and the surface of the nanoparticles rather than physical absorption [22].

The surface capping molecules not only stabilize the nanoparticle in solvents, they also provide potential reaction sites for further modification. As indicated from FT-IR studies, the ligand exchange is incomplete and the surface of the nanoparticles is covered with both AA's and DEG (solvent) molecules. Therefore, the availability of the reaction site is a crucial factor that regulates the chemical concentration in the secondary reaction. Here, ICP-AES was employed to determine the weight percent of iron oxide core and the organic layer, and XPS was applied to provide quantitatively elemental information of surface composition. On the basis of the atomic ratio of carbon and nitrogen, the numbers of surface capping ligands were obtained. As shown in Table 2, except Thr coated nanoparticles, all other five AA functionalized nanoparticles present a similar amount of ligand molecules on the surface with ligand exchange efficiency varied from 27% to 67% for different AA's. We believe that the major cause to this variation is the solubility of the AA's in DEG solvent. As mentioned above, during the ligand exchange process, a new capping ligand will rapidly replace the labile DEG layer and stabilize the nanoparticles in the solvent. Ascribed to the solubility differences, nanoparticles coated by relatively poorly soluble ligand such as Ala and Thr lose their stability in DEG and form precipitates, which prevents further contact with DEG. On the contrary, DEG soluble ligands including Gly, Lys, Arg and Ser stabilize the nanoparticles in the solvents, which prolong the contact of nanoparticles with DEG. The favorable binding of AA's with Fe ions on the surface is unable to fully overcome the competition from excessive amounts of DEG at elevated temperatures. Therefore, the percentages of AA's on the surface of nanoparticles for Ala or Thr are higher than others resulting from the short exchange time and limited contact with competing ligands.

3.3. Colloidal properties

The colloidal stability of the nanoparticles are closely related to their surface chemistry [23,24]. Although the AA's involved in this study are varied in polarity and charge, they all have very good water solubility. The functionalized magnetic nanoparticles are able to form clear solutions either in water or buffer solutions such as saline or PBS buffer without any observable turbidity or precipitate after several months at ambient conditions.

Nanoparticle dispersions with good stability usually have narrow size distribution of hydrodynamic radius (HD) whereas poorly stable dispersions give a broad distribution because of aggregation. Furthermore, HD is an important evaluating factor for employing nanoparticles as therapeutic agents or in clinical diagnostic. Highly polydispersed nanoparticles with large HD only have limited clinical usage. From the DLS measurement (Table 2), nanoparticles with different functionalization show similar values of polydispersity (~0.2) and HD (~13 nm), which were about 6 nm larger than the size observed in TEM. The small HD and good uniformity greatly enhance the possibility of using this kind of functionalized nanoparticles in the development of *in vivo* biomedical applications.

The surface charge can largely affect the stability of the nanoparticle dispersion. AA functionalized nanoparticles appear positive zeta potential under conditions from acidic to lightly basic (Fig. 4), which is ascribed to the positive charge from protonated amine groups in aqueous solution. It is worth mentioning that the observed zeta potentials of Lys and Arg coated nanoparticles are larger than the one from other AA's under the same pH conditions, and the zero value of zeta potentials are also higher than the others. It is because that besides the α-amine group, both Arg and Lys hold additional amine groups which necessarily provide more positively charged group for Colombo repulsion. Furthermore, they are both strong basic natural AA's with much higher isoelectric points than other AA's (pI_{Lys} = 9.59, pI_{Arg} = 11.15). Therefore, it requires stronger basic conditions to neutralize the positive charge and give zero zeta potential.

Since the inter-particle repulsions are mainly generated by coulomb forces, changing the pH value would alter the surface charge and largely affect the colloidal stability. As the pH continuously increasing, deprotonation minimizes the electrostatic interaction, causes aggregation of the nanoparticles and induces turbidity in the colloidal solutions. Interestingly however, zeta potentials of the AA functionalized nanoparticles are extended into negative value range and clear solution can be recovered by the addition of base. As indicated from XPS studies, the surface of the nanoparticles are partially protected by DEG molecules rather than fully covered by AA's. Therefore, the hydroxyl group of DEG will be deportonated and carry a negative charge in strong basic conditions. Thus, the zeta potential of the nanoparticles is also largely depended on the amount of DEG on the surface, which is reflected clearly in the results. Compared to other AA's, Ser and Thr carry additional hydroxyl group that can also be deportonated in basic

Table 2
Colloidal properties and surface capping ligand information on amino acid coated Fe_3O_4 nanoparticles.

Capping ligand	ζ[a] (mV)	HD (nm)	PD (%)	Total no.[b]	No. of AAs[c]	No. of DEG
Ala	25.6	13.7	0.195	1370	685	685
Gly	32	13.4	0.205	1390	428	962
Ser	27	13.1	0.214	1300	347	953
Thr	25	13.2	0.202	1010	673	337
Arg	52	12.9	0.223	1280	427	853
Lys	41	12.4	0.218	1440	480	960

[a] Zeta potential.
[b] Total number of surface capping ligand.
[c] Number of amino acid.

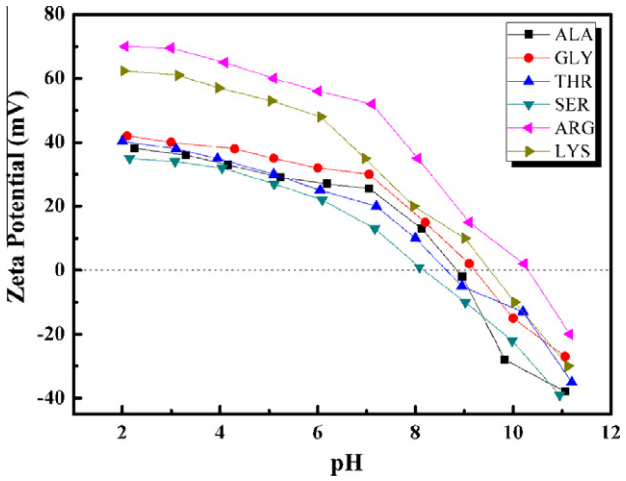

Fig. 4. Zeta potentials of amino acid functionalized nanoparticles as a function of pH value in buffer solutions.

conditions. Consequently, their zeta potentials are able to extend to more basic ranges.

3.4. Magnetic properties

The magnetic properties of AA functionalized nanoparticles were examined by a SQUID magnetometer. Fig. 5 shows the field-cooled (FC) and zero-field-cooled (ZFC) curves of Lys coated nanoparticles. As expected, the product exhibits superparamagnetism with a blocking temperature (T_B) of 74 K which is very close to T_B of other AA functionalized nanoparticles (Table 1). The hysteresis loops also indicate superparamagnetic behavior at room temperature (RT) with no coercivity and remanence, and the saturation magnetization (Ms) is 62 emu g^{-1}. At 5 K, ferromagnetic or ferrimagnetic behavior is observed in Lys functionalized nanoparticles with a coercivity of 272 Oe and a remanence of 13.7 emu g^{-1}. Nanoparticles coated with other AA's show similar values of coercivity, remanence and Ms (Table 1), implying that AA functionalized nanoparticles prepared by this method differ only in surface composition. After removing the organic ligand layer, the normalized Ms are 75.2–78.7 emu g^{-1}, which are very close to the previously reported value of magnetite in similar size [16,25,26].

3.5. Surface reactivity

The surface reactivity of surface functional groups was first tested in polymer conjugation. Under the activation of EDC [27], carboxylic terminated PEG was introduced to react with AA functionalized nanoparticles. Comparing with the FT-IR spectra of AA coated nanoparticles (Fig. 6), an additional peak located at 1730 cm^{-1} appeared after the conjugation with PEG, which is ascribed to the C=O stretching of free carboxylic group, suggesting a successful coupling of PEG with the AA's on the surface of nanoparticles. Additionally, dramatic weight percent increases in the organic layer among all AA functionalized nanoparticles are observed in ICP-AES measurement, which is also attributed to the coupling of large molecular weight PEG.

In light of the affinity of noble metals to amine or thiol groups, the surface reactivity of AA coated nanoparticles were also investigated in a gold nanocrystals attachment test. Solutions containing negative charge stabilized gold nanocrystals were mixed with functionalized iron oxide nanoparticles. After removal of excess gold, UV spectroscopy was first used to study the nanocomposite aqueous solution. However, because of the very low concentration

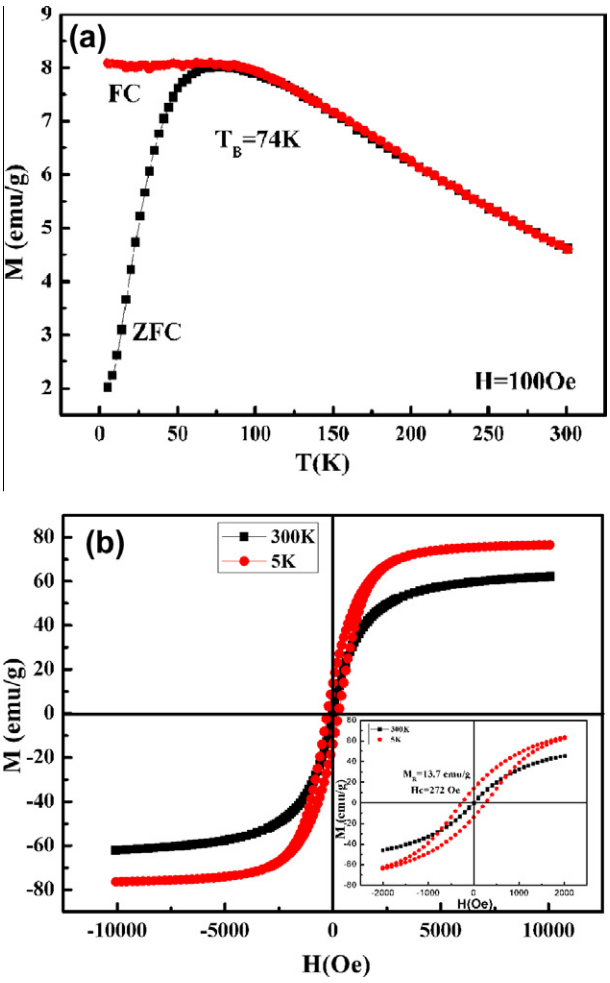

Fig. 5. (a) Temperature dependence of magnetization of Lys-coated Fe_3O_4 under ZFC-FC conditions. (b) Hysteresis loops of Lys-coated Fe_3O_4 at 5 and 300 K.

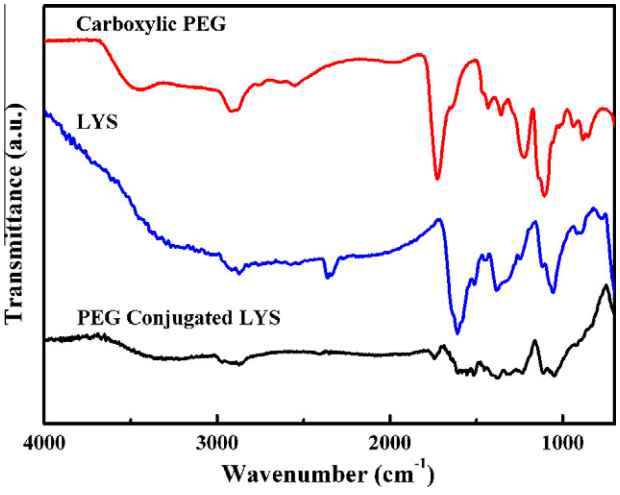

Fig. 6. FT-IR spectra of Lys coated nanoparticles before and after the conjugation with carboxylic terminated PEG.

of gold and strong absorption background of iron oxide, no characteristic plasma band of gold nanoparticles at 520 nm was observed. Alternatively, transmission electron microscopy was applied to verify the present of gold nanocrystals on magnetite. As shown in

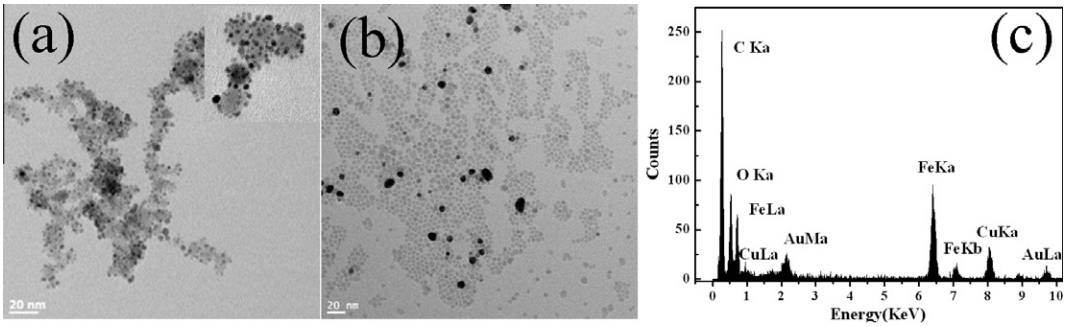

Fig. 7. TEM images of (a) gold nanocrystals attached Lys coated Fe_3O_4 nanoparticles. (b) Residual gold nanocrystals in DEG stabilized Fe_3O_4 nanoparticles. (c) EDS spectra of Au/Fe_3O_4 nanocomposite.

Fig. 7a inset (Fig. S4, Supporting information) small gold nanocrystals (average size of 3 nm) are uniformly attached onto individual iron oxide nanoparticles surface whereas non-functionalized nanoparticles with only DEG coating exhibit a mixture of magnetite and residual amount of gold nanocrystals after washing. High resolution TEM demonstrated that gold nanocrystals are actually docked onto the surface of magnetite nanoparticles rather than simply surrounding them. In contrast, magnetic nanoparticles without surface functionalized were found unable to capture gold nanocrystals to their surface, suggesting that amine groups from the AA's are responsible for the gold attachment. EDS scan was also performed on the nanocomposite. Besides the iron from the nanoparticles and copper from the background, a clear gold peak emerged after the attachment, confirming the elemental composition of the attached nanocrystals. The gold–magnetite nanocomposite was treated with 1 h sonication, and no observable changed was found, illustrating the affinity of amine groups with gold. It is noticed that adding gold nanocrystals affects the dispersibility of all functionalized nanoparticles and induces aggregation. Since the solubility of AA's protected nanoparticles are majorly contributed from the charged functional groups of ligand molecules, consuming the amine groups by attaching gold nanocrystals will reduce electrostatic repulsion and lead to decreased inter-particles separation.

The magnetic properties of PEG functionalized nanoparticles and magnetite–Au nanocomposite were investigated. The saturation magnetization is around 72 emu g^{-1} after normalization to iron oxide, which is very close to the values of AA functionalized nanoparticles before the attachment or reaction, indicating further modification does not have a significant effect on the properties of AA protected nanoparticles.

4. Conclusion

We have demonstrated a simple *in situ* method to prepare AA functionalized magnetic nanoparticles. By using injection techniques at elevated temperature, surface modification was accomplished in a one-pot process, and time consuming post-synthetic ligand exchange reaction can be avoided. The as-prepared products present good crystallinity, uniformity and superior stability in aqueous solution. Because functionalized nanoparticles share the same core materials and differ only in the composition of organic layer, they possess similar magnetic properties. Attachment of noble metal nanocrystals and biocompatible molecules confirm the availability and reactivity of the organic layer, which is crucial for the design and synthesis of complicated multi-functional platforms for clinical applications.

Acknowledgments

This work was supported by a research grant from Louisiana Board of Regents Contract No. LEQSF(2007-12)-ENH-PKSFI-PRS-04. We are indebted to Dr. Baobao Cao for his help in the TEM study and we want to thanks Dr. Daniela Caruntu for useful discussions.

Appendix A. Supplementary material

Supplementary data associated with this article can be found, in the online version, at doi:10.1016/j.ica.2012.01.058.

References

[1] J. Park, M.K. Yu, Y.Y. Jeong, J.W. Kim, K. Lee, V.N. Phan, S. Jon, J. Mater. Chem. 19 (2009) 6412.
[2] K.L. Young, C. Xu, J. Xie, S. Sun, J. Mater. Chem. 19 (2009) 6400.
[3] C. Xu, K. Xu, H. Gu, R. Zheng, H. Liu, X. Zhang, Z. Guo, B. Xu, J. Am. Chem. Soc. 126 (2004) 9938.
[4] T. Hyeon, S.S. Lee, J. Park, Y. Chung, H.B. Na, J. Am. Chem. Soc. 123 (2001) 12798.
[5] S. Sun, H. Zeng, J. Am. Chem. Soc. 124 (2002) 8204.
[6] J. Park, K. An, Y. Hwang, J.-G. Park, H.-J. Noh, J.-Y. Kim, J.-H. Park, N.-M. Hwang, T. Hyeon, Nat. Mater. 3 (2004) 891.
[7] J.A. Dahl, B.L.S. Maddux, J.E. Hutchison, Chem. Rev. 107 (2007) 2228.
[8] C.B. Murray, C.R. Kagan, M.G. Bawendi, Annu. Rev. Mater. Sci. 30 (2000) 545.
[9] M. Lattuada, T.A. Hatton, Langmuir 23 (2006) 2158.
[10] H. Gu, Z. Yang, J. Gao, C.K. Chang, B. Xu, J. Am. Chem. Soc. 127 (2004) 34.
[11] D.K. Kim, M. Mikhaylova, Y. Zhang, M. Muhammed, Chem. Mater. 15 (2003) 1617.
[12] S.-L. Tie, Y.-Q. Lin, H.-C. Lee, Y.-S. Bae, C.-H. Lee, Colloids Surf., A 273 (2006) 75.
[13] Z. Durmus, H. Kavas, M.S. Toprak, A. Baykal, G. Altınçekiç Tuba, A. Aslan, A. Bozkurt, S. Cosgun, J. Alloys Compd. 484 (2009) 371.
[14] G. Marinescu, L. Patron, D. Culita, C. Neagoe, C. Lepadatu, I. Balint, L. Bessais, C. Cizmas, J. Nanopart. Res. 8 (2006) 1045.
[15] D.C. Culita, G. Marinescu, L. Patron, O. Carp, C.B. Cizmas, L. Diamandescu, Mater. Chem. Phys. 111 (2008) 381.
[16] H. Qu, D. Caruntu, H. Liu, C.J. O'Connor, Langmuir 27 (2011) 2271.
[17] D.G. Duff, A. Baiker, P.P. Edwards, Langmuir 9 (1993) 2301.
[18] T. Bala, B.L.V. Prasad, M. Sastry, M.U. Kahaly, U.V. Waghmare, J. Phys. Chem. A 111 (2007) 6183.
[19] J.Y. Park, E.S. Choi, M.J. Baek, G.H. Lee, Mater. Lett. 63 (2009) 379.
[20] K. Nakamoto, Infrared and Raman Spectra of Inorganic and Coordination Compounds, Wiley, New York, 1986.
[21] S. Yu, G.M. Chow, J. Mater. Chem. 14 (2004) 2781.
[22] M. Ma, Y. Zhang, W. Yu, H.-Y. Shen, H.-Q. Zhang, N. Gu, Colloids Surf., A 212 (2003) 219.
[23] A.E. Nel, L. Madler, D. Velegol, T. Xia, E.M.V. Hoek, P. Somasundaran, F. Klaessig, V. Castranova, M. Thompson, Nat. Mater. 8 (2009) 543.
[24] C. Burda, X. Chen, R. Narayanan, M.A. El-Sayed, Chem. Rev. 105 (2005) 1025.
[25] D. Caruntu, G. Caruntu, Y. Chen, C.J. O'Connor, G. Goloverda, V.L. Kolesnichenko, Chem. Mater. 16 (2004) 5527.
[26] D. Caruntu, G. Caruntu, C.J. O'Connor, J. Phys. D: Appl. Phys. 40 (2007) 5801.
[27] G.T. Hermanson, Bioconjugate Techniques, Academic Press, New York, 1996.